Zinc blende and wurtzite CoO polymorph nanoparticles: rational synthesis and commensurate and incommensurate magnetic order

I. V. Golosovsky[a], M. Estrader[b,j,*], A. López-Ortega[c,*], A. G. Roca[b,*], L. López-Conesa[d,e,f], E. Del Corro[b], S. Estradé[e], F. Peiró[d,e], I. Puente-Orench[g,h], J. Nogués[b,i]

[a]*National Research Center "Kurchatov Institute", B.P. Konstantinov Petersburg Nuclear Physics Institute, 188300, Gatchina, Russia.*
[b]*Catalan Institute of Nanoscience and Nanotechnology (ICN2), CSIC and BIST, Campus UAB, Bellaterra, E-08193 Barcelona, Spain.*
[c]*CIC nanoGUNE, Tolosa Hiribidea, 76 E-20018 Donostia-San Sebastian, Spain.*
[d]*LENS-MIND, Departament d'Enginyeria Electrònica i Biomèdica, Universitat de Barcelona, E-08028 Barcelona, Spain.*
[e]*Institute of Nanoscience and Nanotechnology (IN2UB), Universitat de Barcelona, E-08028 Barcelona, Spain.*
[f]*TEM-MAT, CCiT, Universitat de Barcelona, E-08028 Barcelona, Spain.*
[g]*Institut Laue Langevin, 71 avenue des Martyrs, 38000, Grenoble, France.*
[h]*Instituto de Ciencia de Materiales de Aragón, C/Pedro Cerbuna 12, E-50009 Zaragoza, Spain.*
[i]*ICREA, Pg. Lluís Companys 23, E-08010, Barcelona, Spain.*
[j]*Present address: LPCNO, Université de Toulouse, CNRS, INSA, UPS, 135 avenue de Rangueil, 31077 Toulouse, France.*

Abstract

On the nanoscale, CoO can have different polymorph crystal structures, zinc blende and wurtzite, apart from rock salt, which is the stable one in bulk. However, the magnetic structures of the zinc blende and wurtzite phases remain virtually unexplored. Here we discuss some of the main parameters controlling the growth of the CoO wurtzite and zinc blende polymorphs by thermal decomposition of cobalt (II) acetylacetonate. In addition we present a detailed neutron diffraction study of oxygen deficient CoO ($CoO_{0.70-0.75}$) nanoparticles with zinc blende ($\sim$15 nm) and wurtzite ($\sim$30 nm) crystal structures to unravel their magnetic order and its temperature evolution. The magnetic order of the zinc blende nanoparticles is antiferromagnetic and appears at the Néel temperature $T_N \sim 203$ K. It corresponds to the 3-rd type of magnetic ordering in a face-centered cubic lattice with magnetic moments aligned along a cube edge. The magnetic structure in the wurtzite nanoparticles turned out to be rather complex with two perpendicular components. One component is incommensurate, of the longitudinal spin wave type, with the magnetic moments confined in the *ab*-plane. In the perpendicular direction, this magnetic order is uncorrelated, forming quasi-two-dimensional magnetic layers. The component of the magnetic moment, aligned along the hexagonal axis, is commensurate and corresponds to the antiferromagnetic order known as the 2-nd type in a wurtzite structure. The Néel temperature of wurtzite phase is estimated to be $\sim$ 109 K. The temperature dependence of the magnetic reflections confirms the reduced dimensionality of the incommensurate magnetic order. Incommensurate magnetic structures in nanoparticles are an unusual phenomenon and in the case of wurtzite CoO it is probably caused by structural defects (e.g., vacancies, strains and stacking faults).

Keywords: synthesis of nanoparticles, neutron diffraction, incommensurate magnetic structure

1. Introduction

In recent years, there has been an increasing interest in the physical properties of magnetic nanoparticles arising from size reduction. The increase of surface atoms enables the stabilization of crystal structures never seen in the bulk. For CoO, metastable phases with wurtzite and zinc blende (sphalerite) crystal structures, which are polymorphs to the thermodynamically stable CoO with rock salt structure, become stable in nanoparticle form [1, 2, 3]. Wurtzite and zinc blende crystal structures differ by the packing of the characteristic layers and are known for ZnS, MnS and other compounds [4, 5, 6].

Although the CoO with hexagonal wurtzite (W-CoO) and cubic zinc blende (ZB-CoO) crystal structures were reported in the 60's [7], the magnetic order in these compounds has not been established until recently. On the other hand, the long-range magnetic order in nanoparticles of 3d-oxides with rock salt structures, including CoO, is well established [8, 9, 10, 11, 12].

Recently, a renewed interest in the magnetic structure of the CoO wurtzite type nanoparticles has emerged due to the proposed critical role played by this oxide in the ferromagnetic response observed in diluted magnetic semiconductor Co:ZnO films at room temperature [13, 14]. Moreover, in strongly doped Co:ZnO films with Co up to 60 % a short-range, uncompensated antiferromagnetic order has been reported [15].

Density functional theory and Monte Carlo simulations predict either a collinear antiferromagnetic or more complex antiferromagnetic orders for the CoO polymorphs [16, 17, 18, 19, 20]. However, despite extensive studies on nanoparticles and thin films, the magnetic properties of the CoO with wurtzite

and zinc blende structures remain rather controversial. An early neutron diffraction study of CoO nanoparticles with wurtzite crystal structure showed the presence of a weak broad magnetic peak at low temperatures which was associated with a short-range magnetic order [3], in concordance with studies on hexagonal CoO thin films prepared by laser deposition [21]. However, recent neutron diffraction studies have established that both W-CoO and ZB-CoO are antiferromagnetic, although W-CoO exhibits a complex magnetic structure [22].

The lack of a systematic magnetic characterization sets an obstacle for the full understanding and the development of novel applications of these CoO-polymorph structures. Here we present a comprehensive neutron diffraction study to establish the fundamental aspects of the magnetic structures of zinc blende and wurtzite CoO.

2. Experimental

The synthesis of nanostructured CoO with wurtzite and zinc blende phases was carried out by thermal decomposition of cobalt (II) acetylacetonate ($Co(acac)_2$) in 1-octadecene mediated by oleic acid [22]. 19.4 mmol $Co(acac)_2$, 8.8 mmol oleic acid and 20 mL 1-octadecene were combined in a three-neck flask and degassed at room temperature for 30 min. The mix was subsequently heated up to 300 ^{0}C at 3 ^{0}Cmin^{-1} under argon flow and kept at this temperature for 30 min. The reaction was cooled down to room temperature under argon flow. The mixture was washed with toluene and 2-propanol, then centrifuged and finally the sample was dried with a nitrogen flow.

The overall morphology of the sample was characterized by transmission electron microscopy (TEM), using a FEI Tecnai G2 F20 HR(S) TEM microscope operated at 200 kV. The high-angle annular dark-field scanning transmission electron microscopy (HAADF-STEM) images were also acquired using the same microscope. The High Resolution-TEM images were acquired in a JEOL J2100 TEM, equipped with a LaB$_6$ thermionic cathode and operated at 200 kV. The Geometric Phase Analysis (GPA) was carried out using the Digital Micrograph plugin developed by HREM Research Inc.

The CoO nanoparticles were deposited on lacey carbon Cu TEM grids from a hexane suspension. Since the nanoparticles have a lot of organic remains from the synthesis procedure, the TEM grids were heated at 120 ^{0}C for 12 h under ultrahigh vacuum to reduce the organic residue. Finally, the grids were subjected to an argon plasma treatment for 2 min prior to imaging to further reduce the carbonaceous remains.

Neutron powder diffraction was carried out at the D1B beam-line in the Institute Laue-Langevin (Grenoble, France) with a neutron wavelength of 2.524 Å. The X-ray characterization was performed at the BL04-MSPD beam-line on the ALBA Synchrotron (Barcelona, Spain) with a wavelength of 0.4131 Å.

All diffraction patterns were analyzed using the FullProf suit [23]. In the calculations of the line-shape, the Thompson-Cox-Gastings approximation was used [24].

The Raman spectra were registered with a WiTec spectrometer, using an excitation wavelength of 488 nm with a 0.2 mW power to avoid sample heating and phase transformation. A 1800 gr/nm grating was chosen to provide a proper spectral resolution and deconvolution of the Raman peaks present in the 400 to 700 cm^{-1} spectral range.

3. Results

3.1. Synthesis

It is well-known that the cubic rock salt structure is the most stable CoO phase. Namely, although the decomposition of cobalt precursors often leads to a zinc blende intermediate (which is the least stable polymorph) [25], if the synthesis follows a thermodynamic regime the most stable structure, i.e., rock salt CoO, is formed (Figure 1a). For example, thermal decomposition carried out at moderate temperatures for the synthetic approach (i.e., around 200 ^{0}C) is enough to promote the formation of single rock salt CoO nanoparticles [26]. However, under kinetic conditions, set by the chemical parameters (precursor concentration, solvents or surfactants) and the reaction conditions (heating rate, stabilization temperature, reflux temperature or time), it is possible to form and stabilize the two other metastable polymorph CoO phases: hexagonal wurtzite and cubic zinc blende (Figure 1b,c) [25].

Interestingly, the growth of either wurtzite or zinc blende CoO nanoparticles is mediated by the formation of a zinc blende nuclei intermediate (which is controlled to a certain extent by the chemical parameters) [27]. This transformation is controlled by an energy barrier which is set by the primary zinc blende CoO size. In fact, there is a critical zinc blende radius, where the energy barrier is low enough to enable the nucleation of the wurtzite phase (see Figure 1b,c) [28]. If the zinc blende CoO intermediate is large (e.g., in solid state reactions, for instance, by annealing Co-acetate at high temperatures) [7] the final phase is zinc blende, since the energy barrier to transform zinc blende CoO into wurtzite CoO is very high (Figure 1b). Namely, even adjusting the reactions conditions (heating rate, stabilization temperature, reflux temperature or time) wurtzite would be disfavored (Figure 1b). However, if the zinc blende intermediate is small (i.e., below the critical radius), by using a low precursor concentration or if the energy of the system is high (e.g., such as reflux temperatures around 300 ^{0}C or above) the energy barrier for the wurtzite formation can be surpassed, allowing the formation of wurtzite nanoparticles (Figure 1c).

Thus, within this framework, subtle changes in the reaction parameters lead to the formation of different phases. In fact, in contrast to solid-state routes, there are no reports on the synthesis of pure zinc blende nanoparticles by thermal decomposition in liquid media, whereas the synthesis of single wurtzite nanoparticles has been achieved [1, 2]. This suggests that surfactants lower the critical size enabling the complete transformation from zinc blende to wurtzite.

For the synthesis of CoO by the thermal decomposition of cobalt acetylacetonate, important reaction parameters such as the precursor concentration, nature of the solvent, surfactants, heating rate and temperature reaction will determine the final CoO phase composition. For example, changing the reaction

temperature by merely 50 ^{0}C (from 250 ^{0}C and 300 ^{0}C) has a strong effect on the final structure. At 250 ^{0}C, the main phase is zinc blende with a small amount of rock salt. Nevertheless, the final product at 300 ^{0}C is a mixture of zinc blende and wurtzite (see Figure 2a). Namely, at 250 ^{0}C, as it can be inferred from the peak widths, the zinc blende nanoparticles have not grown sufficiently to transform into wurtzite so they tend to form the rock salt phase. However, at 300 ^{0}C, there is enough thermal energy to grow larger zinc blende nanoparticles enabling the transformation to wurtzite.

On the other hand, the ratio between wurtzite and zinc blende in the final product can be controlled by the polarity of the solvent. Namely, 1-octadecene is a non-polar solvent with less co-ordinating capacity than benzyl ether, thus affecting the growth regime of CoO. When 1-octadecene is used as solvent an equal mixture of wurtzite and zinc blende is obtained. However, when benzyl ether is used the proportion of zinc blende is considerably larger than in the case of 1-octadecene (see Figure 2b). Non-coordinative 1-octadecene enables a fast growth regime leading to larger sizes of zinc blende while in the case of benzyl ether the increase in coordination slows down the growth of zinc blende nanoparticles leading to a poorer transformation to wurtzite. The nature of the ligands also affects the growth regime. Oleic acid and oleylamine are common surfactants in thermal decomposition synthesis and especially in the CoO system. However, they have a different role in the reaction since oleic acid, and also its deprotonated form, oleate, favours the formation of zinc blende and wurtzite mixtures. Conversely, the use of oleylamine slows down the particle growth favouring a thermodynamic regime, leading to the formation of pure rock salt CoO nanoparticles (see Figure 2c). Finally, the initial amount of Co(acac)$_2$ has also a strong effect on the final product. When the initial amount of Co(acac)$_2$ is very small virtually pure either zinc blende or wurtzite particles can be obtained, although the quantities obtained are rather small (Figure 2d). However, increasing the initial mass of Co(acac)$_2$ results always in mixed zinc blende-wurtzite products. Note that obtaining a pure wurtzite phase is somewhat difficult since it requires a certain particle size of the pre-formed zinc blende phase, which is not straightforward to control.

Since the objective of this work is to carefully study the magnetic structure of both phases and neutron diffraction experiments can easily discriminate the contribution of the two phases, we have chosen the synthesis route that leads to a larger quantity of material, especially wurtzite, since neutron diffraction experiments require some hundreds of mg. It is worth emphasizing that having a large amount of sample is critical to obtain high quality neutron diffraction patterns.

As can be seen in the TEM and STEM images (Figures 3a,b), the sample consists of triangular-shaped nanoparticles (Figure 3d) of around 40 nm in edge (Figure 3c), which corresponds to wurtzite phase with a hexagonal crystal symmetry [7] and smaller zinc blende particles of around 15 nm (Figure 3c) with more irregular spheroidal shape (Figure 3e) [28]. Moreover, the TEM characterization evidences that, in fact, many of the wurtzite-CoO particles exhibit clear defects, as can be seen in Figure 4a-4e. A more careful analysis of the defects was car-ried out by Geometric Phase Analysis (GPA). The phase map obtained by GPA for the most intense spot in the fast Fourier transform (FFT) (Figure 4f) (i.e., the (100) reflection of the wurtzite phase) shows a sign change when crossing the line of the defect (Figure 4g-4j). This implies that the continuity of the crystal planes is interrupted. The quality of the images (due to the remaining carbonaceous residue) does not allow determining the exact nature of the structural defects.

3.2. X-ray and neutron diffraction.

The XRD pattern shows the characteristic reflections from the W-CoO and ZB-CoO phases (Figure 5a). The refined unit cell parameters are $a = 4.5534(1)$ Å for the cubic zinc blende crystal structure and $a = 3.2526(1)$ Å; $c = 5.1977(1)$ Å for the hexagonal wurtzite crystal structure [22]. The values in brackets correspond to the errors (i.e., estimated standard deviation). The zinc blende and wurtzite phases are 37 % and 63 % of the whole sample volume, respectively. No traces of CoO rock salt or metallic Co impurities were detected. The fit of the neutron powder diffraction renders similar structural parameters.

The form and dimensions of the nanoparticles, as well as the inner stresses, can be determined from the peak broadening $\Delta Q(Q)$. Indeed, the contribution arising from the finite size of the particles is Q-independent, while the inner stresses give a contribution proportional to the moment transfer Q. However, as can be seen from the difference pattern in Figure 5a, the profiles of the diffraction peaks are not properly described in the frame of a standard refinement. Nevertheless, the profile refinement can be strongly improved using an independent refinement of every reflection width, known as "Pawley" or "matching mode" approach (Figure 5b). This refinement allows defining $\Delta Q(Q)$ more precisely. In Figure 6, the Q-dependence of the refined $\Delta Q(Q)$ is shown for the two types of nanoparticles.

3.2.1. Zinc blende CoO nanoparticles.

It can be seen in Figure 6 that the zinc blende nanoparticles have a $\Delta Q(Q)$ which does not follow a monotonic dependence. This indicates a strong anisotropic shape of the nanoparticles. The non-monotonic dependence of the peak broadening implies an "anisotropic size-effect", which is characteristic for diffraction of nanoparticles, whose shape cannot be well approximated by a sphere [29, 30]. In this case, the "apparent size", i.e. the nanoparticle dimension along the scattering vector [31], differs even for the reflections with the same interplanar distance. Power averaging leads to an irregular behavior of the peak broadening ΔQ, with moment transfer (or diffraction angle).

The estimation from the XRD patterns using the Scherrer formula gives a characteristic average size for the ZB-CoO nanoparticles of 13.0(5) nm, in agreement with the TEM results [22].

In neutron scattering the scattering lengths of oxygen and cobalt are comparable; therefore the profile refinement allows us to evaluate the relative occupancies of O and Co atoms. The refined values for zinc blende nanoparticles correspond to the

chemical formula $CoO_{0.7(1)}$, which indicates a strongly non-stoichiometric compound with a significant amount of oxygen vacancies [22].

The comparison of the neutron diffraction patterns measured at 300 and 10 K reveals a strong magnetic contribution at low temperatures, as shown by the difference pattern in Figure 7. From the nuclear reflections positioned at large momentum transfer, one can precisely define the lattice parameters of the comprising nanoparticles and hence to calculate the positions of the magnetic reflections, based on the cubic structure (SG $F\bar{4}3m$) for zinc blende nanoparticles and hexagonal structure (SG $P6_3mc$) for wurtzite nanoparticles.

The observed magnetic reflections reveal for ZB-CoO nanoparticles a simple commensurate magnetic order, which corresponds to the 3-rd type of antiferromagnetic ordering in an face-centered cubic (fcc) lattice with the wave vector $\mathbf{k} = [0.5\ 0\ 0]$ [32]. Such type of magnetic order is typical for zinc blende type compounds [4, 33] (Figure 8). The magnetic moments of 2.3(2) μ_B/ion are aligned along a cube edge [22].

The temperature dependence of the intensity of the characteristic reflection (0.5 1 0) is well fitted by a straight line (Figure 9a). Using a power law $I \sim (T - T_N)^{2\beta}$, this means a critical exponent $\beta = 0.5$, which corresponds to a mean field behaviour [34]. The fit renders a Néel temperature (T_N) of ZB-CoO, $\sim$ 203(5) K, in concordance with the T_N estimated from magnetic measurements [22].

3.2.2. Wurtzite CoO nanoparticles.

In contrast to the ZB-CoO nanoparticles, the nanoparticles with wurtzite structure demonstrate a monotonic increase of ΔQ with Q (Figure 6), indicating they have an isotropic shape, but also present inner stresses.

The slope of the $\Delta Q(Q)$ curve indicates the presence of microstrains, which originate from the presence of defects with long-ranged strain fields like planar defects [35].

Additionally, the sample was characterized using Raman spectroscopy. The results (Figure S1) are consistent with hexagonal CoO spectra in the literature [36]. However, some of the observed Raman peaks are slightly shifted and broader with respect to the reported values, which may indicate the presence of residual stress and defects in the sample. Moreover, the higher spectral resolution used in our measurements reveals a deconvolution of several Raman peaks.

The estimation from the peak broadening gives a characteristic size for the W-CoO nanoparticles of 32.0(5) nm. Note that the somewhat smaller size with respect to the TEM values is probably related to presence of defects in the W-CoO structure (see Figure 4) The refined occupancies of the O and Co atoms correspond to the chemical formula $CoO_{0.75(6)}$. Thus, similar to the ZB-CoO nanoparticles, W-CoO is strongly non-stoichiometric with a considerable amount of oxygen vacancies [22].

For a description of the magnetic order in the wurtzite crystal structure, it is more convenient, instead of the hexagonal unit cell, to use the orthohexagonal unit cell for which $a = a'$, $b = \sqrt{3}a'$ $c = c'$, where the primed symbols refer to the original

hexagonal cell. All the reflections for the wurtzite nanoparticles are indexed using this type of unit cell.

To describe the observed magnetic pattern in the W-CoO nanoparticles we first assumed a wave vector $\mathbf{k} = [0\ 0.5\ 0]$, which corresponds to the magnetic cell, which is the double of the chemical one along the b-direction, similar to the one reported for other compounds with wurtzite structure [4, 5, 6]. However, we could not describe the positions of all observed reflections, magnetic and nuclear, in the frame of a unique hexagonal or orthogonal unit cell. The analysis shows that the only way to index the reflections is adopting an incommensurate magnetic structure in the wurtzite nanoparticles. In this case the refined wave vector is $\mathbf{k} = [0\ 0.457(1)\ 0]$ and, thus, the strongest reflection has indexes (1 0.46 0) [22].

The analysis of the observed reflections from the incommensurate structure in the wurtzite lattice shows that the observed magnetic order corresponds to the 4-th type antiferromagnetic structure, in contrast to the 3-rd type magnetic order reported for other compounds with a wurtzite structure (after L. Corliss [4]). In the 3-rd type magnetic order, the nearest moments are antiparallel, while in the 4-th type they are parallel [4].

In magnetic scattering, only the component of the magnetic moment that is perpendicular to the diffraction vector is being measured [37]. Therefore, the extinction of the reflection (0 0.46 0) in W-CoO indicates that the magnetic moments are aligned along the b-axis in the basal plane. This implies that the observed incommensurate magnetic structure belongs to the longitudinal spin wave (LSW) type or spin density wave (Figure 10a).

In the experimental diffraction pattern, only the reflections with indexes hk0 are observed. Such extinction is characteristic of the two-dimensional magnetic order in the ab-plane, with h and k indexes only. The quasi-two-dimensional order suggests that magnetic correlations exist within a thin layer parallel to the basal plane.

On the other hand, a lack of correlations in the direction perpendicular to the basal plane assumes a sharp boundary in the magnetic order along the c-axis. Such arrangement can be described by a form-factor of $sin(Qx)/Qx$, whose "zeros" are approximately at the positions of the reflections with $l \neq 0$. This form-factor is a Fourier transform of a "rectangular pulse", which in our case corresponds to a layer with a thickness of $2x$. A simple calculation results in a layer thickness of $\sim$ 6.8 Å, i.e., the correlation length along the c-axis is about 1-2 unit cell parameters.

Importantly, in the case of the LSW, the spin direction is rigidly defined. Therefore, the lack of correlations between different layers along the c-axis can result from the lack of phase relations between the spin waves associated with different atoms in a cell. Consequently, the observed unusual structure is a peculiarity of incommensurate LSW.

In the low-temperature pattern from the wurtzite nanoparticles, apart from the superstructure antiferromagnetic reflections, there is a magnetic contribution into the nuclear reflection (1 1 0). This contribution can be attributed to a ferromagnetic as well as an antiferromagnetic order with $\mathbf{k} = [0\ 0\ 0]$. The analysis demonstrates that the observed magnetic contribution

to the nuclear reflections can be explained by an antiferromagnetic structure of the 2-nd type in the wurtzite crystal structure [4] with the magnetic moments aligned along the c-axis (Figure 10b) [22], i.e., perpendicular to the magnetic moments, which form the incommensurate, quasi-two-dimensional order in the basal plane.

The profile refinement gives magnetic moments of 2.8(2) μ_B/ion and 1.4(1) μ_B/ion for the two perpendicular components, incommensurate and commensurate, respectively [22]. The total moment is 3.1(1) μ_B/ion. This volume-averaged magnetic moment is substantially smaller than the moment 3.80(1) μ_B/ion found for bulk, rock salt, CoO [38]. This effect is a common phenomenon and it is explained by the moment disorder at the surface of a nanoparticle. Interestingly, this phenomenon has been observed in nanostructured CoO and MnO, embedded into porous media [8, 9, 10].

Importantly, no ferromagnetic contribution was observed in the neutron diffraction pattern. Moreover, note that due to the lack of long range order, the uncompensated spins observed in magnetization and dichroism measurements [22] cannot be detected by our neutron diffraction experiments and any diffuse scattering due to short-range ordered spins is beyond of the accuracy of our measurement.

The temperature-dependence of the intensity of the characteristic reflections can render additional information (Figure 9b). First, it is seen that the reflection from the incommensurate structure and the contribution to nuclear reflection have the same Néel temperature, $T_N \sim 109(1)$ K, indicating that, indeed, they belong to the same wurtzite lattice. Second, the critical exponent β for the incommensurate structure, calculated from the magnetic reflection (1 0.46 0), is noticeably smaller, $\beta = 0.28(3)$ compared to the $\beta = 0.5$ (mean-field approximation) for the commensurate component, which gives a contribution into the nuclear reflection (1 1 0). This implies a reduced dimensionality of the incommensurate magnetic order [39] and consequently a quasi-two-dimensional character of the magnetic order, in concordance with the previous analysis.

Hence, instead of a simple Néel-type commensurate magnetic structure with $\mathbf{k}$ = [0 0.5 0], known for bulk materials with a wurtzite structure, in W-CoO nanoparticles the magnetic order is more complex. There are two perpendicular components with different magnetic order: an incommensurate component with the wave vector $\mathbf{k}$ = [0 0.457(1) 0], correlated within a thin layer parallel to the basal plane, and a component along the c-axis with the wave vector $\mathbf{k}$ = [0 0 0] with a simple antiferromagnetic structure (Figure 10).

As can be seen in Figure S2, the resulting profile refinement, including both ZB-CoO and W-CoO phases, presents an excellent agreement with the experiment.

4. Discussion

It should be noted that an incommensurate magnetic order in nanoparticles is a rather unusual phenomenon. Remarkably, incommensurate magnetic order has been detected reliably by the neutron diffraction in three systems, in 20 nm nanoparticles of ε-Fe$_2$O$_3$ [40], in nanoparticles of CoCrFe$_2$O$_4$ with 10-50 nm size [41] and in CoCr$_2$O$_4$ [42].

The incommensurate order, observed in the CoO wurtzite nanoparticles, has a pronounced two-dimensional character, which is most probably caused by the defects in the anisotropic wurtzite crystal structure. It is worth emphasizing, that in the previous neutron study of CoO wurtzite nanoparticles only short-range magnetic order was observed, which was explained by the frustrated super-exchange in the wurtzite lattice [3, 21]. However, the structural defects (e.g., vacancies, strains or planar defects) could release the frustration and provide the observed long-range, two-dimensional order that we observe [43]. Thus, the amount and type of defects in W-CoO probably determine its macroscopic magnetic behavior [22]. In fact, this could shed light on the spread of magnetic behaviour reported for W-CoO [1, 2, 3, 21, 22].

In addition, since W-CoO may nucleate on growth faults of ZB-CoO nuclei [27], the resulting planar defects in W-CoO could, in fact, influence the two-dimensional character of its magnetic order.

CoO is traditionally considered as a classical example of a compound with a large orbital moment. Therefore, its magnetic behavior should fit the predictions of the three-dimensional Ising model with a critical exponent β = 0.312 (or 5/16). However, the commensurate component in CoO with wurtzite and zinc blende structures demonstrates the usual, "mean-field" behavior, with $\beta \sim 0.5$. Such an increase of the critical exponent could be a size-effect known as the "rounding" of a phase transition, which results from the correlation length being limited by the nanoparticle size [9, 39].

Another possible source for the "rounding" of the phase transition could be a mutual interaction of wurtzite and zinc blende nanoparticles with different magnetic orders due to a well-developed interface between them. For example, magnetic proximity effects [30, 44, 45] between ZB-CoO, with a higher Néel temperature, and W-CoO could induce a magnetic order in the W-CoO. However, our neutron diffraction experiments with single phase wurtzite nanoparticles showed that although the diffraction signal was too weak to perform any quantitative calculations, the long-range magnetic order was unambiguously observed. This implies that the magnetic order in the zinc blende CoO nanoparticles with higher Néel temperature cannot be responsible for the long-range magnetic order in wurtzite CoO nanoparticles, which is obviously intrinsic. However, some mutual influence cannot be ruled out completely.

5. Conclusion

The main parameters affecting the growth of the growth of the CoO wurtzite and zinc blende polymorphs by thermal decomposition of cobalt (II) acetylacetonate (temperature, polarity of the solvent, surfactants, and amount of precursor) have been established.

Moreover, neutron diffraction studies were performed in CoO nanoparticles with wurtzite (~30 nm) and zinc blende (~15 nm) crystal structures to establish their elusive magnetic

order. The magnetic order in the zinc blende nanoparticles was found to be commensurate, antiferromagnetic, corresponding to the 3-rd type of magnetic ordering in an fcc lattice with the magnetic moment aligned along a cube edge, similar to other compounds with a zinc blende structure.

In contrast to the zinc blende CoO nanoparticles, the magnetic structure in the wurtzite CoO nanoparticles turned out to be complex with two perpendicular components. One component is incommensurate, of the longitudinal spin wave type. It has a pronounced two-dimensional order correlated within thin layers (1-2 unit cells) parallel to the basal plane. The temperature dependence of the incommensurate component confirms its two-dimensional character. The perpendicular component of the magnetic moment, along the hexagonal axis, is commensurate, with an antiferromagnetic order known as the 2-nd type in a wurtzite structure. No ferro or ferrimagnetic ordering was detected.

The unusual incommensurate magnetic structure is probably caused by the different types of defects present in the anisotropic crystal structure of wurtzite on the nanoscale.

5.1. Data availability

The raw/processed data required to reproduce these findings cannot be shared at this time due to technical or time limitations.

7. Appendix A. Supplementary data

Supplementary data associated with this article can be found, in the online version, at

References

[1] W. S. Seo, J. H. Shim, S. J. Oh, E. K. Lee, N. H. Hur and J. T. Park, Phase- and size-controlled synthesis of hexagonal and cubic CoO nanocrystals, J. Am. Chem. Soc. 127 (2005) 6188-6189, http://dx.doi.org/10.1021/ja050359t.

[2] K. An, N. Lee, J. Park, S. C. Kim, Y. Hwang, J. G. Park, J. Y. Kim, J. H., Park, M. J. Han, J. Yu, and T. Hyeon, Synthesis, characterization, and self-assembly of pencil-shaped CoO nanorods, J. Am. Chem. Soc. 128 (2006) 9753-9760, http://dx.doi.org/10.1021/ja0608702.

[3] A. S. Risbud, L. P. Snedeker, M. M. Elcombe, A. K. Cheetham and R. Seshadri, Wurtzite CoO, Chem. Mater. 17 (2005) 834-838, http://dx.doi.org/10.1021/cm0481269.

[4] L. Corliss, N. Elliott and J. Hastings, Magnetic structures of the polymorphic forms of manganous sulfide, Phys. Rev. 104 (1956) 924-928, https://doi.org/10.1103/PhysRev.104.924.

[5] T. M. Giebultowicz, J. J. Rhyne, J. K. Furdyna, and U. Debska, Neutron diffraction study of the wurtzite structure dilute magnetic semiconductor $Zn_{0.45}Mn_{0.55}Se$, J. Appl. Phys. 61 (1987) 3540-3542, http://dx.doi.org/10.1063/1.338717.

[6] B. Van Laar, H. M. Rietveld and D. J. W. Ijdo, Magnetic and crystallographic structures of Me_xNbS_2 and Me_xTaS_1, J. Sol. State Chem. 3 (1971) 154-160, https://doi.org/10.1016/0022-4596(71)90019-3.

[7] M. J. Redman, E. G. Steward, Cobaltous oxide with the zinc blende/wurtzite-type crystal structure, Nature 193 (1962), 867-867, https://doi.org/10.1038/193867a0.

[8] I. V. Golosovsky, I. Mirebeau, G. André, D. A. Kurdyukov, Yu. A. Kumzerov, and S. B. Vakhrushev, Magnetic ordering and phase transition in MnO embedded in a porous glass, Phys. Rev. Lett. 86 (2001) 5783-5786, http://dx.doi.org/10.1103/PhysRevLett.86.5783.

[9] I. V. Golosovsky, I. Mirebeau, V. P. Sakhnenko, D. A. Kurdyukov, and Y. A. Kumzerov, Evolution of the magnetic phase transition in MnO confined to channel type matrices: neutron diffraction study, Phys. Rev. B: Condens. Matter 72 (2005) 144409, http://dx.doi.org/10.1103/PhysRevB.72.144409.

[10] I. V. Golosovsky, I. Mirebeau, G. André, M. Tovar, D. M. Tobbens, D. A. Kurdyukov, Yu. A. Kumzerov, Magnetic phase transition in a nanostructured antiferromagnet CoO embedded in porous glass, Phys. Solid State 48 (2006) 2130-2133, http://dx.doi.org/10.1134/S1063783406110151.

[11] M. Estrader, A. López-Ortega, I. V. Golosovsky, S. Estradé, A. G. Roca, G. Salazar-Alvarez, L. López-Conesa, D. Tobia, E. Winkler, J. D. Ardisson, W. A. A. Macedo, A. Morphis, A. M. Vasilakaki, K. Trohidou, A. Gukasov, I. Mirebeau, O. Makarova, R. D. Zysler, F. Peiró, M. D. Baró, L. Bergstrom, J. Nogués, Origin of the large dispersion of magnetic properties in nanostructured oxides: Fe_xO/Fe_3O_4 nanoparticles as a case study, Nanoscale 7 (2015) 3002-3011, http://dx.doi.org/10.1039/c4nr06351a.

[12] López-Ortega, D. Tobia, E. Winkler, I. V. Golosovsky, G. Salazar-Alvarez, S. Estradé, M. Estrader, J. Sort, M. A. González, S. Suriñach, J. Arbiol, F. Peiró, R. D. Zysler, M. D. Baró and J. Nogués, Size-dependent passivation shell and magnetic properties in antiferromagnetic/ferrimagnetic core/shell MnO nanoparticles, J. Am. Chem. Soc. 132 (2010) 93989407, http://dx.doi.org/10.1021/ja1021798.

[13] T. Dietl, T. Andrearczyk, A. Lipińska, M. Kiecana, Maureen Tay, and Yihong Wu, Origin of ferromagnetism in $Zn_{1x}Co_xO$ from magnetization and spin-dependent magnetoresistance measurements, Phys. Rev. B: Condens. Matter 76 (2007) 155312, https://doi.org/10.1103/PhysRevB.76.155312.

[14] M. Venkatesan, C. B. Fitzgerald, J. G. Lunney and J. M. D. Coey, Anisotropic ferromagnetism in substituted zinc oxide, Phys. Rev. Lett. 93 (2004) 177206, https://doi.org/10.1103/PhysRevLett.93.177206.

[15] V. Ney, B. Henne, J. Lumetzberger, F. Wilhelm, K. Ollefs, A. Rogalev, A. Kovacs, M. Kieschnick, A. Ney, Coalescence-driven magnetic order of the uncompensated antiferromagnetic Co doped ZnO, Phys. Rev. B 94 (2016) 224405, https://doi.org/10.1103/PhysRevB.94.224405.

[16] T. Archer, R. Hanafin and S. Sanvito, Magnetism of CoO polymorphs: density functional theory and Monte Carlo simulations, Phys. Rev. B: Condens. Matter 78 (2008) 014431, http://dx.doi.org/10.1103/PhysRevB.78.014431.

[17] R. Hanafin, T. Archer, and S. Sanvito, Magnetism of wurtzite CoO nanoclusters, Phys. Rev. B: Condens. Matter 81 (2010) 054441, http://dx.doi.org/10.1103/PhysRevB.81.054441.

[18] M. J. Han, H.-S. Kim, D. G. Kim, and J. Yu, Collinear and noncollinear spin ground state of wurtzite CoO, Phys. Rev. B: Condens. Matter 87 (2013) 184432, http://dx.doi.org/10.1103/PhysRevB.87.184432.

[19] M. Y. Yin, X. C. Wang, W. B. Mi, G. F. Chen, B. H. Yang, A first-principles prediction on the magnetism in CoO with Co and O vacancies, J. Alloy Compd. 610 (2014), 422-427, http://dx.doi.org/10.1016/j.jallcom.2014.05.040.

[20] R. I. Hines, N. L. Allan, G. S. Bell and W. C. Mackrodt, An ab initio HartreeFock study of the magnetic states of the polymorphs of MnS, J. Phys.: Condens. Matter 9 (1997) 7105-7118.

[21] J. Alaria, N. Cheval, K. Rode, M. Venkatesan and J . M. D. Coey, J. Phys. D: Appl. Phys. 41 (2008) 135004, http://dx.doi.org/10.1088/0022-3727/41/13/135004.

[22] A. G. Roca, I. V. Golosovsky, E. Winkler, A. López-Ortega, M. Estrader, R. D. Zysler, M. D. Baró, and J. Nogués, Unravelling the elusive antiferro-

magnetic order in wurtzite and zinc blende CoO polymorph nanoparticles, Small 14 (2018) 1703963, http://dx.doi.org/10.1002/smll.201703963.

[23] J. Rodriguez-Carvajal, Recent advances in magnetic structure determination by neutron powder diffraction, Physica B: Physics of Condensed Matter, 192 (1993), 55-69; http://dx.doi.org/10.1016/0921-4526(93)90108-I; http://www.ill.eu/sites/fullprof.

[24] P. Thompson, D. Cox, and B. Hastings, Rietveld refinement of Debye-Scherrer synchrotron X-ray data from Al_2O_3, J. Appl. Crystallogr. 20 (1987) 79-83, https://doi.org/10.1107/S0021889887087090

[25] R. W. Grimes, A. N. Fitch, Thermal decomposition of cobalt(II) acetate tetrahydrate studied with time-resolved neutron diffraction and thermogravimetric analysis, J. Mater. Chem. 1 (1991) 461-468, https://doi.org/10.1039/JM9910100461.

[26] A. V. Ravindra, B. C. Behera, P. Padhan, O. I. Lebedev, W. Prellier, Tailoring of crystal phase and Néel temperature of cobalt monoxides nanocrystals with synthetic approach conditions. J. Appl. Phys. 116 (2014) 033912, http://dx.doi.org/10.1063/1.4890512.

[27] R. W. Grimes, K. P. D. Lagerlöf, Polymorphs of cobalt oxide, J. Am. Ceram. Soc. 74 (1991) 270-273, https://doi.org/10.1111/j. 1151-2916.1991.tb06873.x.

[28] F. Huang, J. F. Banfield, Size-dependent phase transformation kinetics in nanocrystalline ZnS, J. Am. Chem. Soc. 127(12) (2005) 4523-4529, http://dx.doi.org/10.1021/ja048121c.

[29] A. López-Ortega, M. Estrader, G. Salazar-Alvarez, S. Estradé, I. V. Golosovsky, R. K. Dumas, D. J. Keavney, M. Vasilakaki, K. N. Trohidou, J. Sort, F. Peiró, S. Suriñach, M. D. Baró, and J. Nogués, Strongly exchange coupled inverse ferrimagnetic soft/hard, $Mn_xFe_{3-x}O_4/Fe_xMn_{3-x}O_4$, core/shell heterostructured nanoparticles, Nanoscale, 4 (2012) 5138-5147, http://dx.doi.org/110.1039/c2nr30986f.

[30] I. V. Golosovsky, S. B. Vakhrushev, J. L. García-Muñoz, M. Brunelli, W.-M. Zhu, Z.-G. Ye, and V. Skumryev, Neutron diffraction study of the $(BiFeO_3)_{1x}(PbTiO_3)_x$ solid solution: nanostructured multiferroic system, J. of Phys.: Condens. Matter, 27 (2015) 046004, http://dx.doi.org/10.1088/0953-8984/27/4/046004.

[31] J. I. Langford and D. Löer, Powder diffraction, Rep. Prog. Phys, 59 (1996) 131-234.

[32] J. S. Smart, Effective field theories of magnetism, W. B. Saunders Co., Philadelphia-London, 1966.

[33] Tapan Chatterji (Ed.), Neutron scattering from magnetic materials, Elsevier B.V., 2006.

[34] L. D. Landau and E. M. Lifshitz,The classical theory of fields, Pergamon Press, 1971.

[35] M.A. Krivoglaz, Theory of X-Ray and thermal-neutron scattering by real crystals, Plenum, New York, 1969.

[36] A.V. Ravindra, B.C. Behera, P. Padhan, Laser Induced Structural Phase Transformation of Cobalt Oxides Nanostructures. J. Nanosci. Nanotechnol. 14 (2014) 5591, http://dx.doi.org/10.1166/jnn.2014.9023.

[37] Yu. A. Izyumov, V. E. Naish, R. P. Ozerov, Neutron diffraction of magnetic materials, Plenum Publishing, New York, 1991.

[38] M. D. Rechtin, S. C. Moss, and B. L. Averbach, Influence of lattice contraction on long-range order in CoO near T_n, Phys. Rev. Lett. 24 (1970) 1485-1489, https://doi.org/10.1103/PhysRevLett.24.1485.

[39] Y. Imry, Finite-size rounding of a first-order phase transition, Phys. Rev. B: Condens. Matter, 21 (1980) 2042-2043, https://doi.org/10.1103/PhysRevB.21.2042.

[40] M. Gich, C. Frontera, A. Roig, E. Taboada, E. Molins, H. R. Rechenberg, J. D. Ardisson and W. A. A. Macedo, C. Ritter, V. Hardy, J. Sort, V. Skumryev and J. Nogués, High- and Low-Temperature Crystal and Magnetic Structures of ϵ-Fe_2O_3 and their correlation to its magnetic properties, Chem. Mater. 18 (2006) 3889-3897, https://doi.org/10.1021/cm060993l.

[41] D. Kumar, J. K. Galivarapu, A. Banerjee, K. S. Nemkovski, Y. Su and C. Rath, Size dependent magnetic transitions in $CoFe_{0.1}Cr_{1.9}O_4$ nanoparticles studied by magnetic and neutron polarisation analysis, Nanotechnology 27 (2016) 175702, https://doi.org/10.1088/0957-4484/27/17/175702.

[42] D. Zákutná, J. J. Vlček, P. Fitl, K. Nemkovski, D. Honecker, D. Nižňanský, and S. Disch, Noncollinear magnetism in nanosized cobalt chromite, Phys. Rev. B, 98 (2018) 064407, https://doi.org/10.1103/PhysRevB.98.064407.

[43] A. P. Ramirez, Strongly Geometrically Frustrated Magnets, Annu. Rev. Mater. Sci. 24 (1994) 453-480, https://doi.org/10.1146/annurev.ms.24.080194.002321.

[44] I. V. Golosovsky, G. Salazar-Alvarez, López-Ortega, M. A. González, J. Sort, M. Estrader, S. Suriñach, M. D. Baró, and J. Nogués, Magnetic proximity effect features in antiferromagnetic/ferrimagnetic core-shell nanoparticles, Phys. Rev. Lett. 102 (2009) 247201, https://doi.org/10.1103/PhysRevLett.102.247201.

[45] J. A. de Toro, D. P. Marques, P. Muñiz, V. Skumryev, J. Sort, D. Givord, and J. Nogués, High temperature magnetic stabilization of cobalt nanoparticles by an antiferromagnetic proximity effect, Phys. Rev. Lett. 115 (2015) 057201, https://doi.org/10.1103/PhysRevLett.115.057201.
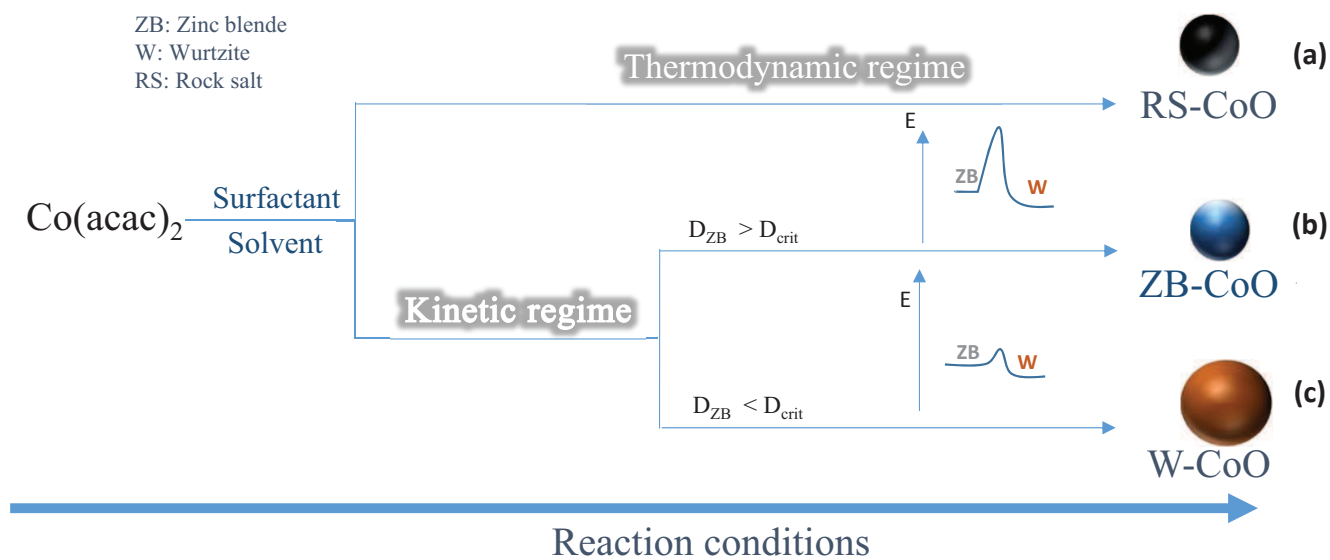
Figure 1: Synthesis of the different CoO polymorphs as a function of the reaction regime. (a) Under a thermodynamic regime the most stable polymorph (rock salt CoO) is formed. If the reaction follows a kinetic regime, the final phase depends on the diameter of the primary zinc blende CoO nanoparticles. (b) When the diameter is larger than a critical dimeter, it is possible to stabilize the zinc blende CoO phase because the reaction conditions cannot provide sufficient energy to overcome the energy barrier to lead to the wurtzite polymorph. (c) Below a critical diameter, the energy barrier is much lower and the conversion to wurtzite CoO phase is possible by adjusting the reaction conditions.
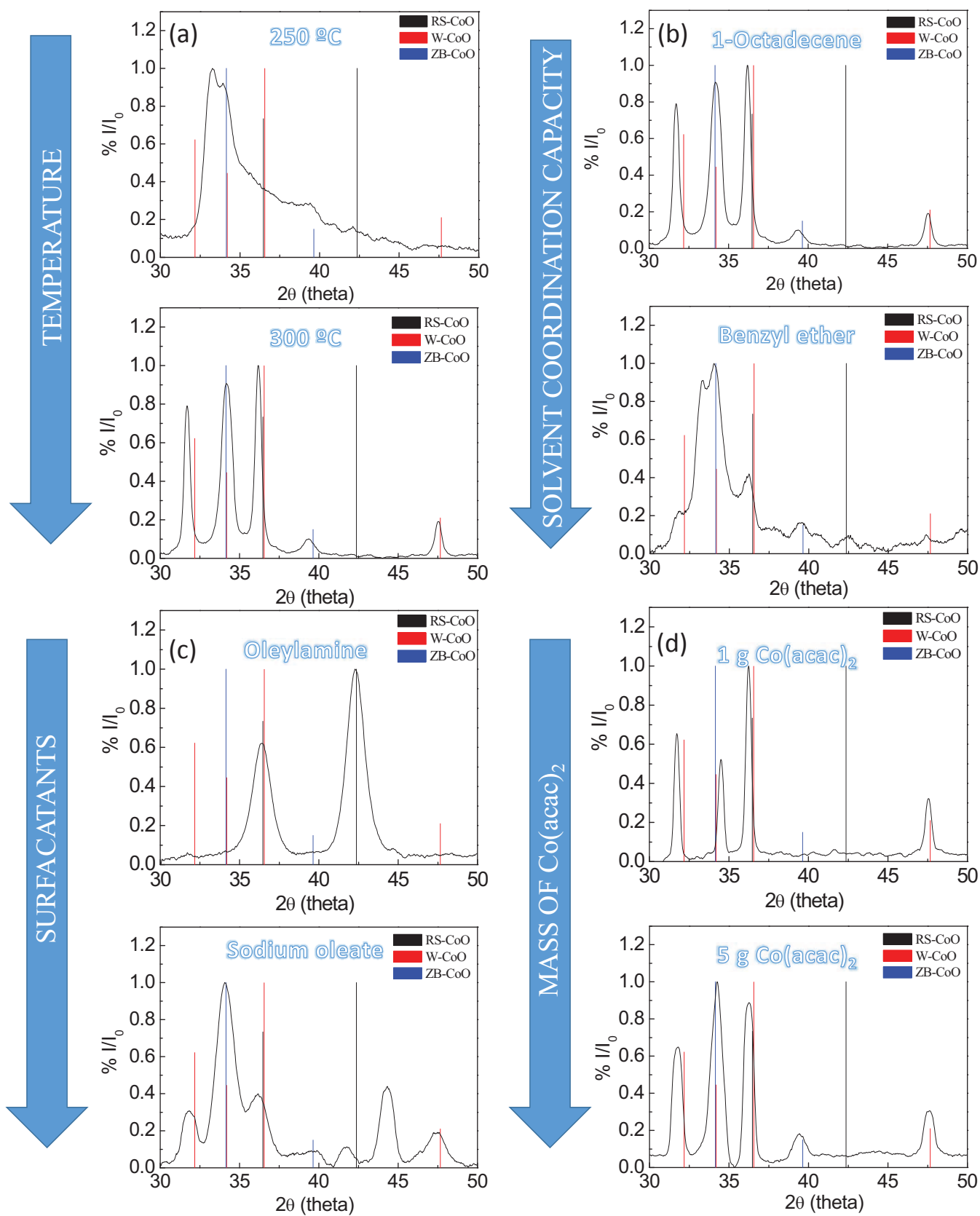
Figure 2: X-Ray diffraction patterns of the CoO nanoparticles synthesized in different conditions; (a) at different temperatures; (b) in solvents with different coordination capacity, (c) with different surfactants, (d) with different amount of Co(acac)$_2$.
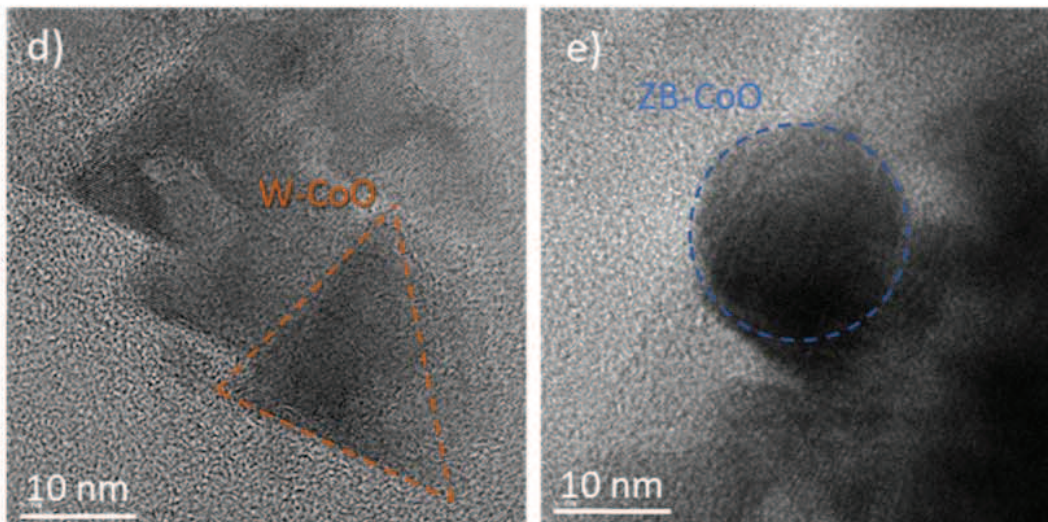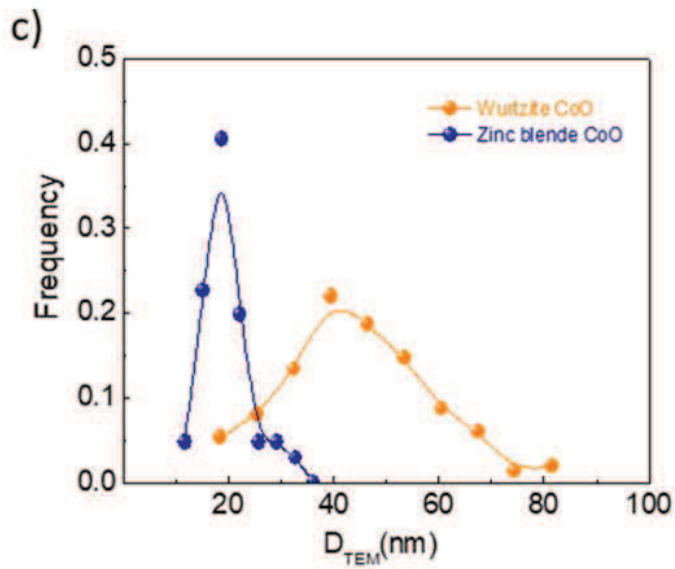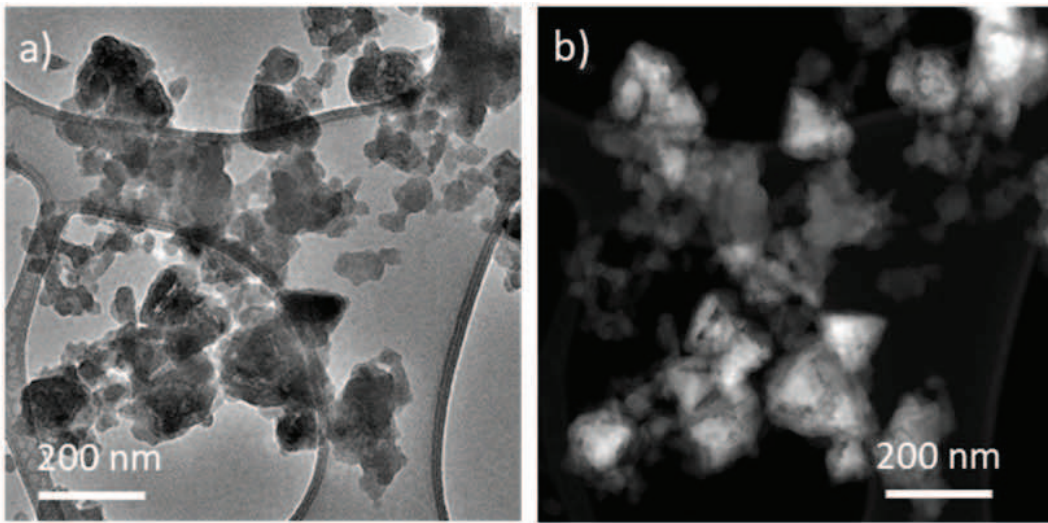
Figure 3: (a) TEM and (b) HAADF-STEM images of the CoO sample with mixed wurtzite and zinc blende CoO particles. Note that since the wurtzite particles are larger than the zinc blende ones, they appear brighter in the HAADF-STEM image. (c) Particle size distribution of the CoO particles. (d) Single wurtzite particle highlighted in orange (e) Single zinc blende CoO particle highlighted in blue. 10
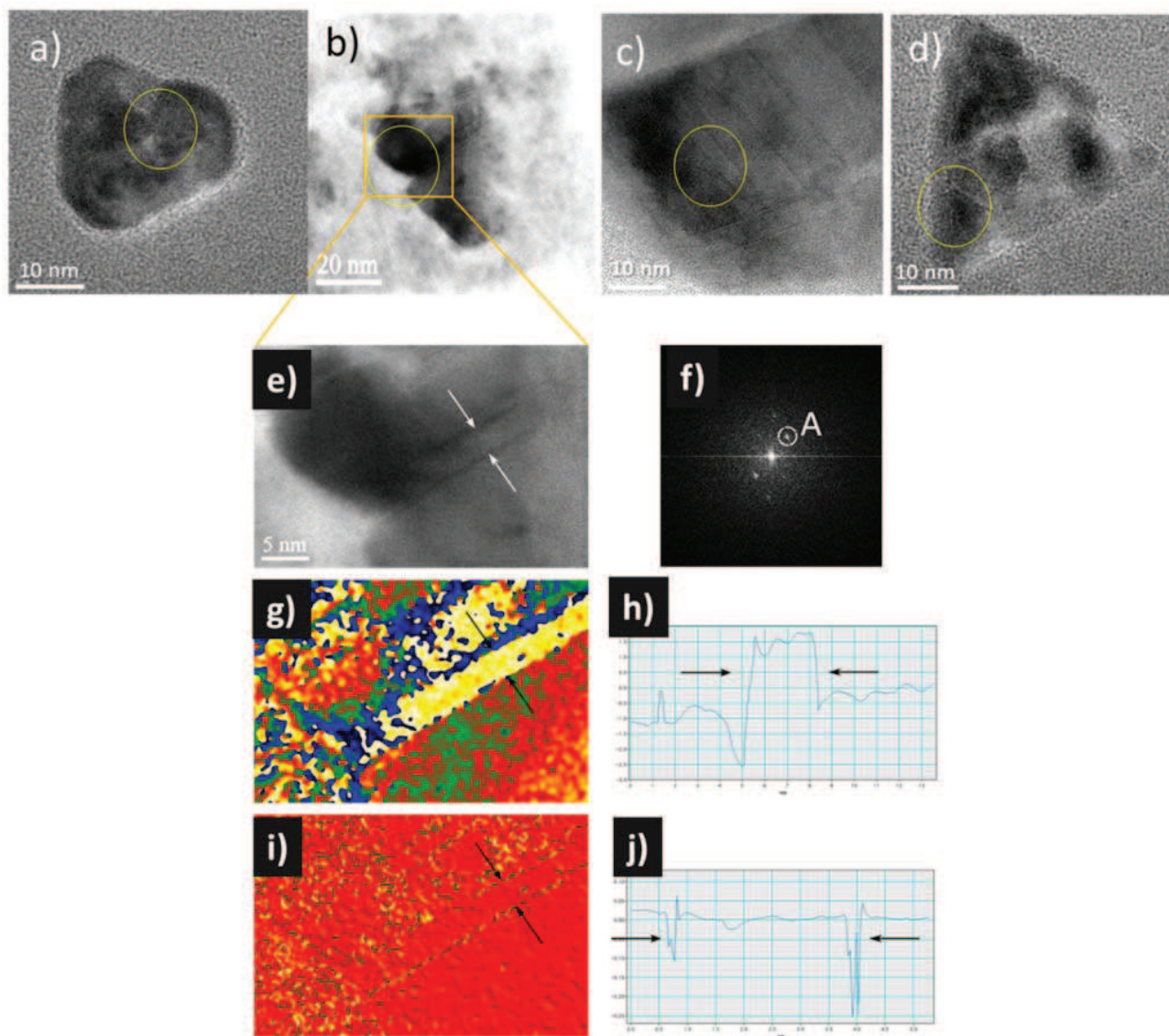
Figure 4: a-d) Different single CoO nanoparticles, where planar defects have been highlighted by circles. e) HRTEM image of the marked area of the particle shown in b) and f) its corresponding FFT. g) Phase map from the reflection A highlighted in the FFT in panel f. h) Line profile of the phase map crossing the two line defects. i) Strain map from the same area and j) line profile of the strain map showing the two line defects.
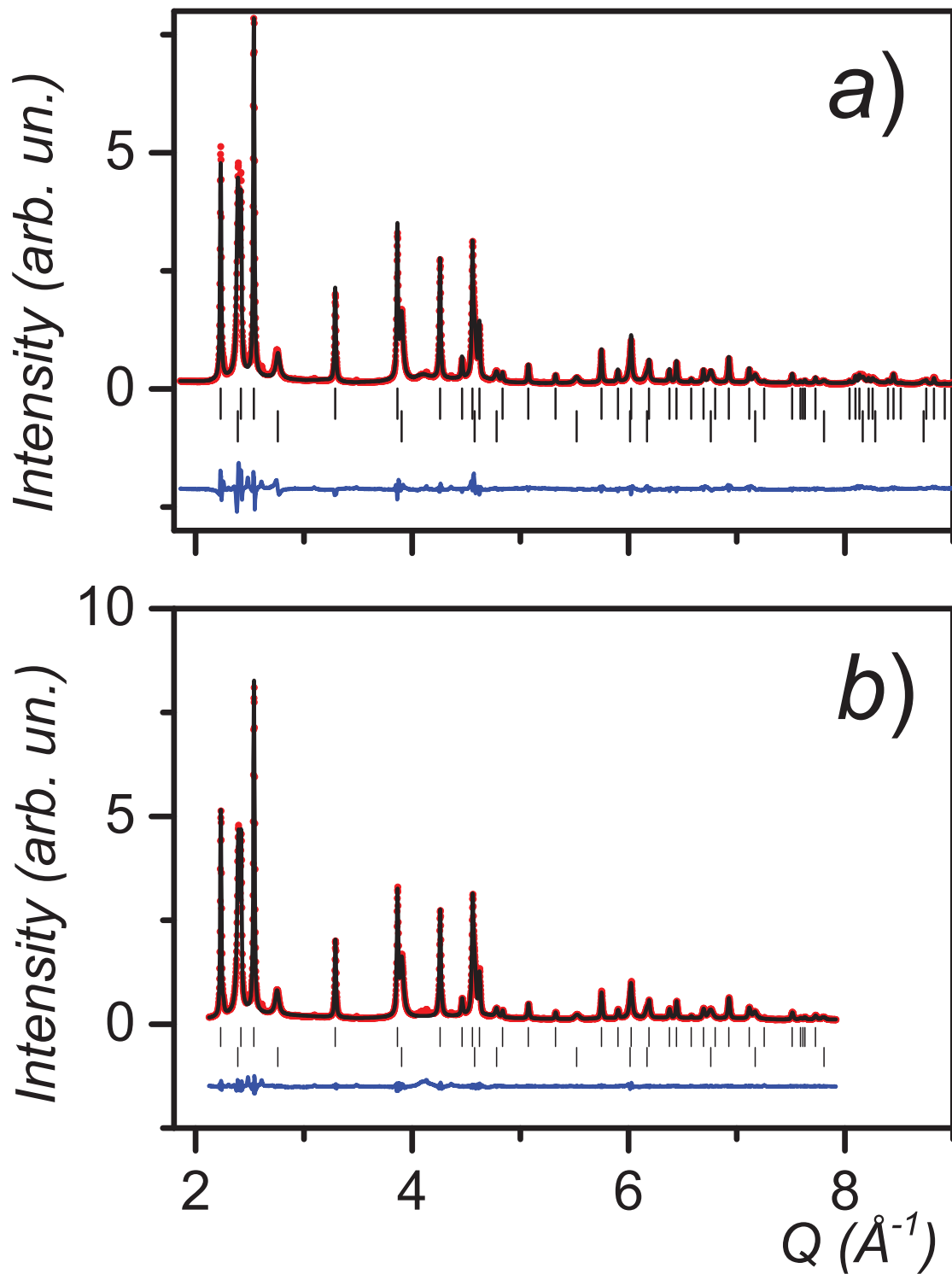
Figure 5: Profile refinement of the XRD-pattern using the standard isotropic model (a) and individual fit of the full width at half maximum for every reflection i.e., "Pawley" or "matching mode" type refinement (b). The experimental points are shown in red symbols, the calculated profile with a black line, and the difference pattern with a blue line. The bars indicate the positions of reflections, where the top row corresponds to the wurtzite structure and the bottom row to the zinc blende structure.
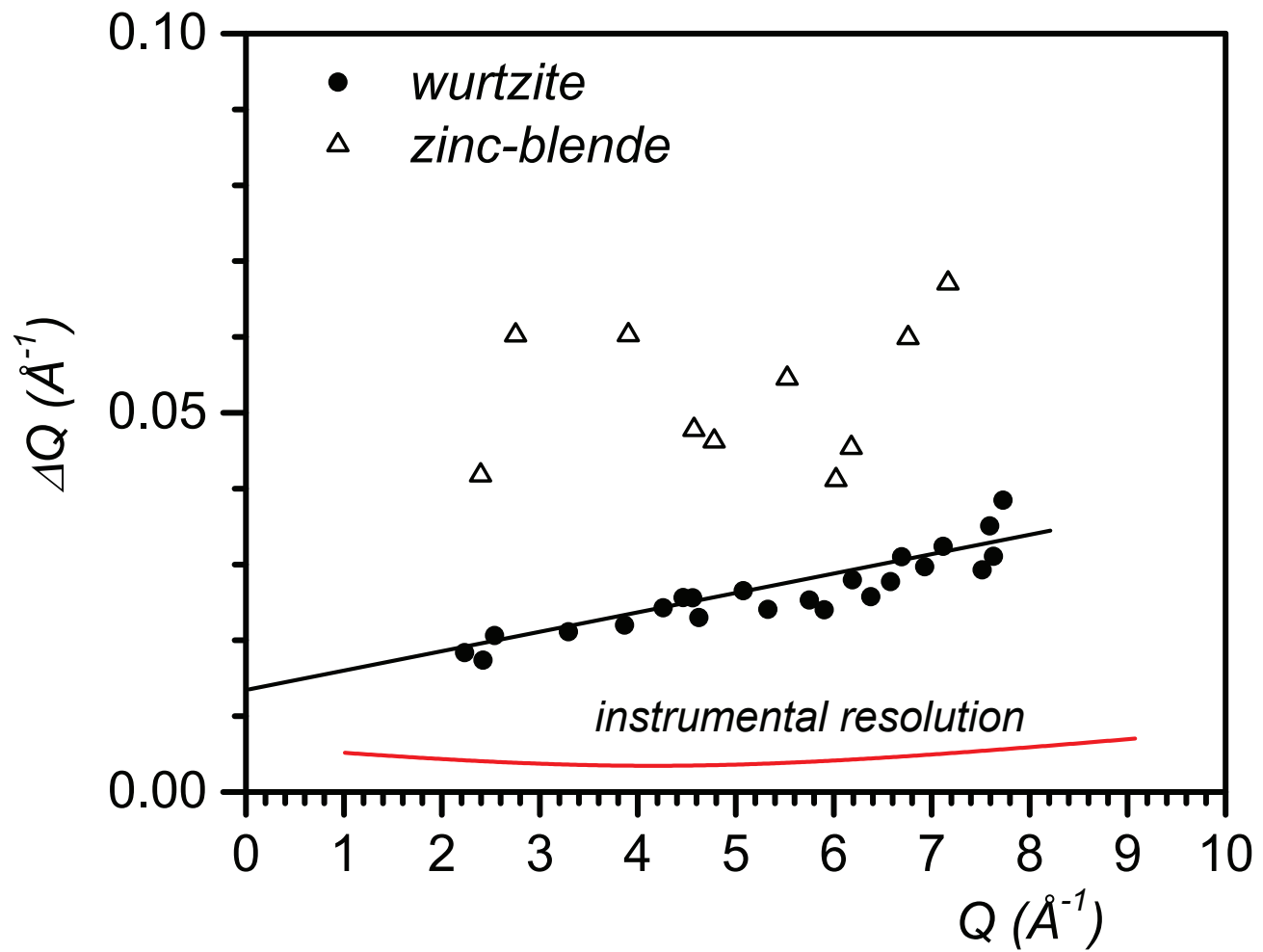
Figure 6: Refined peak broadening ΔQ vs. momentum transfer Q (full analogue of the Williamson-Hall plot) for the wurtzite (solid circles), (the black line is a linear fit) and zinc blende (open triangles) nanoparticles. The red line is the instrumental resolution.
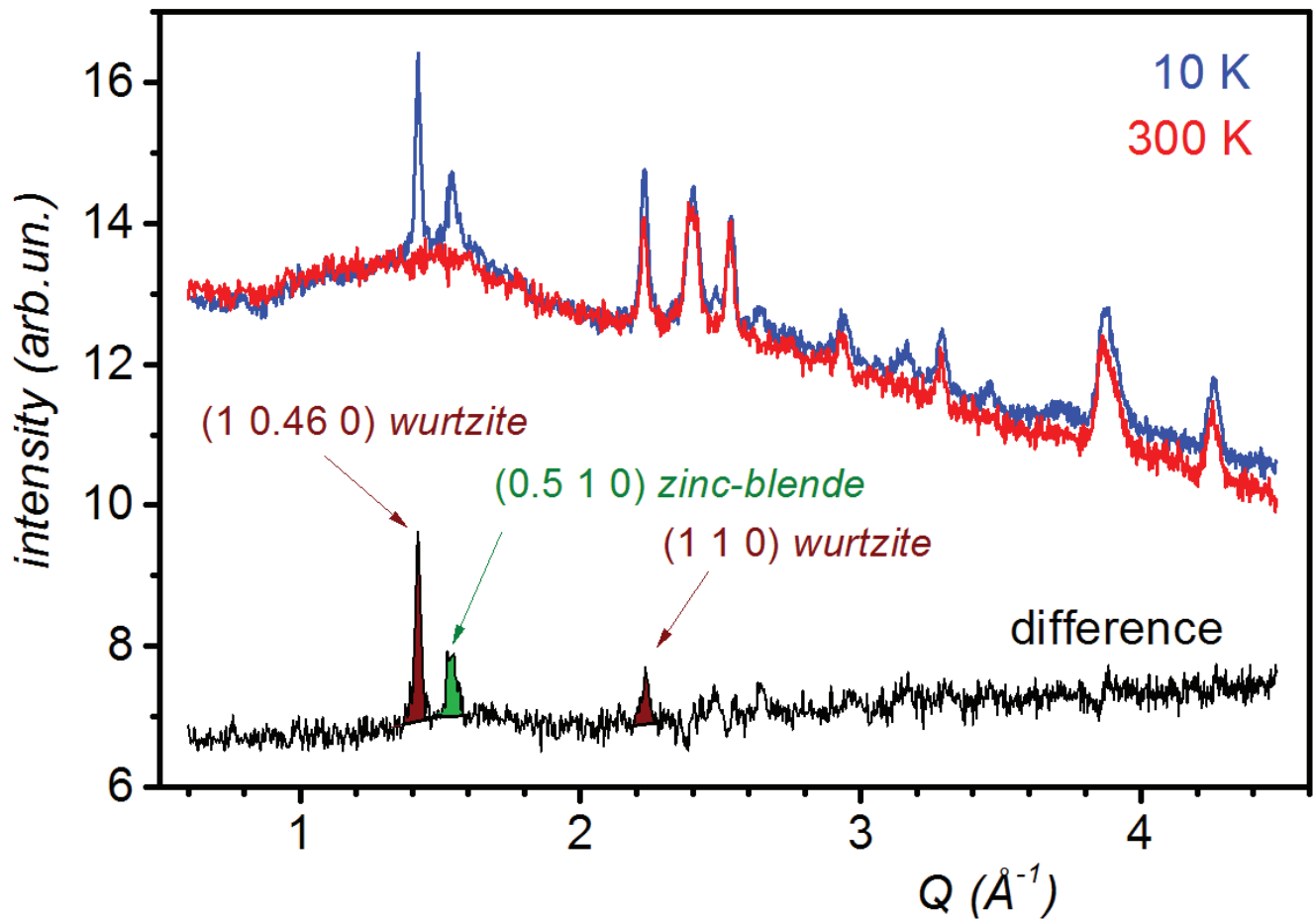
Figure 7: Neutron diffraction patterns measured at 300 K (in red), at 10 K (in blue) and the difference pattern (in black). The indexes of the characteristic magnetic reflections are given in the difference pattern.
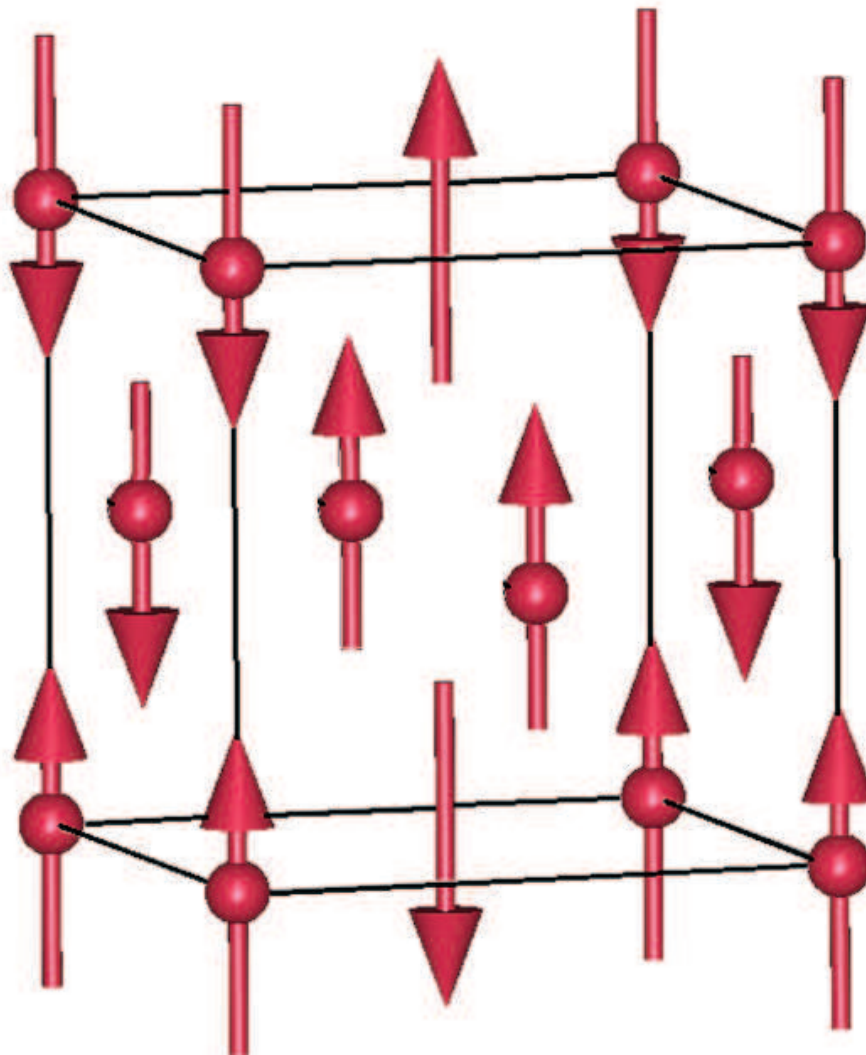
Figure 8: Antiferromagnetic structure in the zinc blende-CoO nanoparticles, which corresponds to the 3-rd type structure in a face-centered cubic lattice.
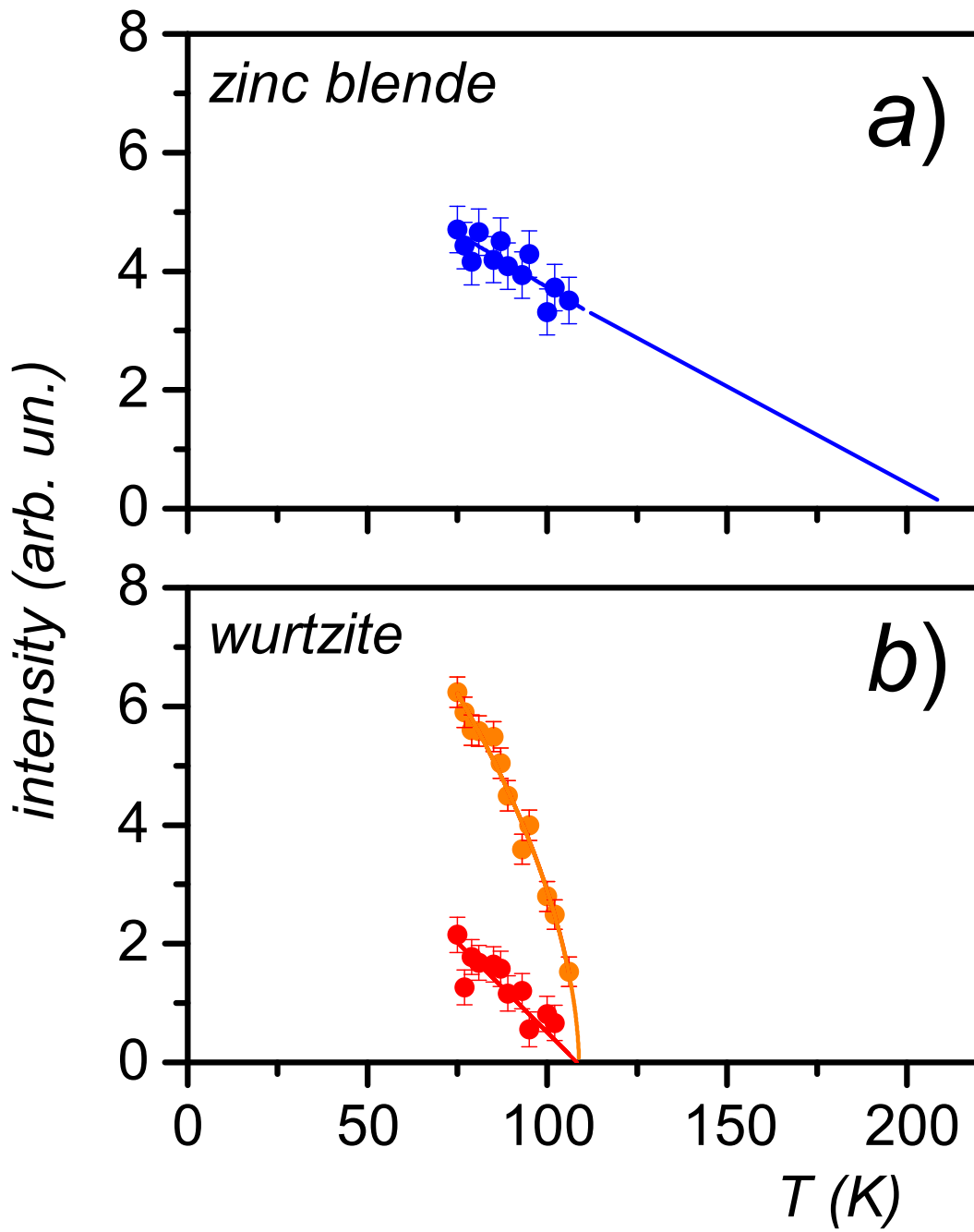
Figure 9: (a) Temperature dependence of the characteristic (0.5 1 0) reflection for the zinc blende nanoparticles. (b) Temperature dependence of the (1 0.46 0) reflection for the incommensurate order (in orange) and of the (1 1 0) reflection for the commensurate component (in red) for the wurtzite nanoparticles. Solid lines are fits to a power law $(T - T_N)^{2\beta}$, where β is the critical exponent. (See text for details.)
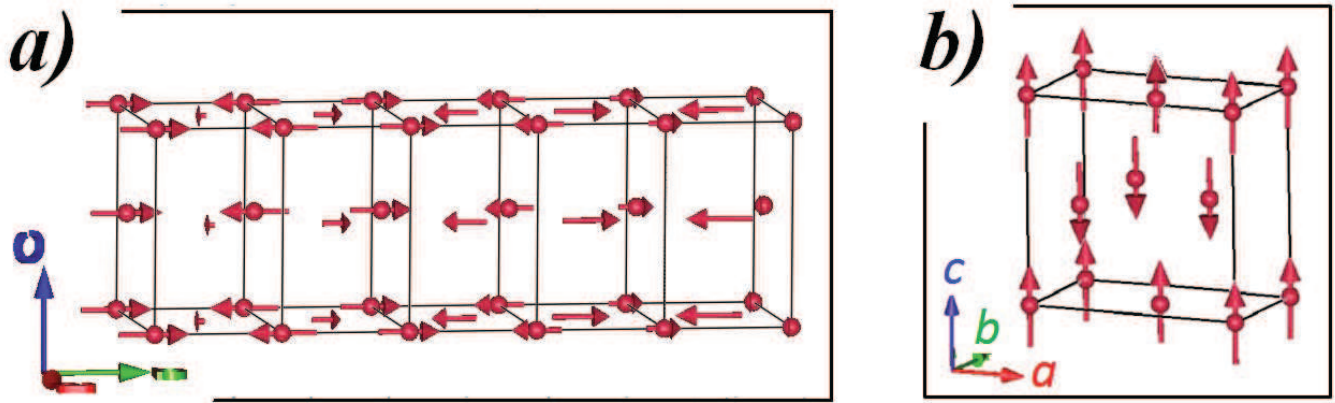
Figure 10: Magnetic structures of the wurtzite-CoO nanoparticles: (a) incommensurate order in the *ab*-plane and (b) commensurate order along the *c*-axis.